Received: November 30, 2022. Revised: February 6, 2023.

INASS

International Journal of
Intelligent Engineering & Systems

http://www.inass.org/

Heuristic Approach on Robot Formation to Find a Gas Leak Source

Dony Hutabarat[1] Muhammad Rivai[1]* Muhammad Agung Nursyeha[2]
Djoko Purwanto[1] Sheva Aulia[3]

[1]*Department of Electrical Engineering, Institut Teknologi Sepuluh Nopember, Surabaya, Indonesia*
[2]*Department of Electrical Engineering, Institut Teknologi Kalimantan, Balikpapan, Indonesia*
[3]*Department of Information Systems, Institut Teknologi Sepuluh Nopember, Surabaya, Indonesia*
* Corresponding author's Email: muhammad_rivai@ee.its.ac.id

Abstract: Robots have been widely used to overcome problems in the environment. In this case, mobile robots were used to find the source of gas leakage. Each robot was equipped with gas sensors in the form of a stereo-nose and Light Detection and Ranging (LiDAR). The robot formation in finding the gas leak source had the advantage of expanding the gas detection area, meaning the robots could not easily lose the pathway. However, detecting through formation required a longer execution time. To speed up the robots in finding the gas leak source's location, this study involved the heuristic model. This model allowed each robot to change positions in a formation. The experiment results showed that the robot group using the heuristic model was 62.2% faster than a single robot. This method was also 19.4% faster than the robot group with a fixed formation.

Keywords: Environment, Gas leak source, Gas sensors, Heuristic model, LiDAR, Mobile robots.

NOMENCLATURE

x, y	Position in Cartesian space	$\dot{\gamma}_f$	Rotation speed in formation
β	Gas concentration	$\dot{\varphi}_{res}$	Resultant motion speed
β_r	Gas concentration on the right sensor	$\dot{\gamma}_{res}$	Resultant rotation speed
β_l	Gas concentration on the left sensor	$\|d\|$	Robot distance
$\Delta\beta$	Gas concentration change	$\Delta\|d\|$	Change in robot distance
ω_l	Left motor speed	α	The angle between target and the robot's orientation
ω_r	Right motor speed	$\Delta\alpha$	Change in angle between target and robot's orientation
φ	Robot position	χ_k^i	Position and orientation of robot i at time k
γ	Robot orientation	$\dot{\chi}_k^i$	The robot's movement speed
$\dot{\varphi}$	Motion speed	r_i	Distance in polar coordinate
$\dot{\gamma}$	Rotation speed	θ_i	Angle in polar coordinate
$\dot{\varphi}_g$	Motion speed toward the gas source	r_l	Left encoder
$\dot{\gamma}_g$	Rotation speed toward the gas source	r_r	Right encoder
$\dot{\varphi}_f$	Motion speed in formation	R	Electrical resistance

1. Introduction

Gas leak source detection by robots is a compelling research topic because of its security and automatic aspects, despite having high difficulties. Various methods and test scenarios were carried out to analyze the robots' behavior in finding gas leak sources in environments similar to actual conditions

[1-3]. The search for gas leak sources by robots becomes important when toxic and flammable gases are involved. The gas can endanger humans in terms of health and life [4].

A multi-robot system has many advantages compared to a single robot, as it can solve several problems faster, and more accurately [5]. The heuristic approach is widely used to solve problems in various fields by producing optimal solutions [6-7]. The heuristic approach in robots has been applied to finding gas leak sources with minimum gas tracking time [2]. In using the heuristic approach, each robot will exchange information in the form of fitness value and position [3]. Determining robot positions with cameras and communication among robots becomes a problem when the robot's scope gets bigger [2], [3]. Moreover, localization by spreading robots in any place produces a less optimal tracking process. When a change in the propagation or gas plume direction arises, the robots in the group can easily lose the gas concentration.

The formation is an egression for tracking gas leak sources where there is a change in the plume. Formations make for wider gas detection than a single robot [8]. Formation behavior mimics group intelligence, especially in birds that fly in groups in a V formation.

The heuristic approach in gas tracking formation is defined by the existence of a leader robot and its followers [9]. A leader robot can be replaced by its follower if the detected gas concentration is lower. Thus, the group of robots can carry out the tasks within the minimum amount of time and none of them will lose their way.

This paper will further discuss how to design a robot, stereo-nose, and robot speed control; implementation of the heuristic approach in the robot formation to find a gas leak source; and how the robots can exchange information about the amount of gas concentration in accordance with their positions. In the results and analysis section, stereo-nose experiments are discussed, as well as robot group testing in tracking with various scenarios, namely independent, tracking with fixed formation, and tracking with heuristic approaches in the formation. In addition, the gas leak source search approach performance is compared. Further tracking experiments were carried out in the presence of gas or odor plume disrupters.

This paper was organized as follows: section 1 briefly reviews some related literature on this topic; section 2 explains the details of the proposed model algorithm; section 3 presents the experiment results and its analysis; section 4 offers conclusions and an idea for future work.

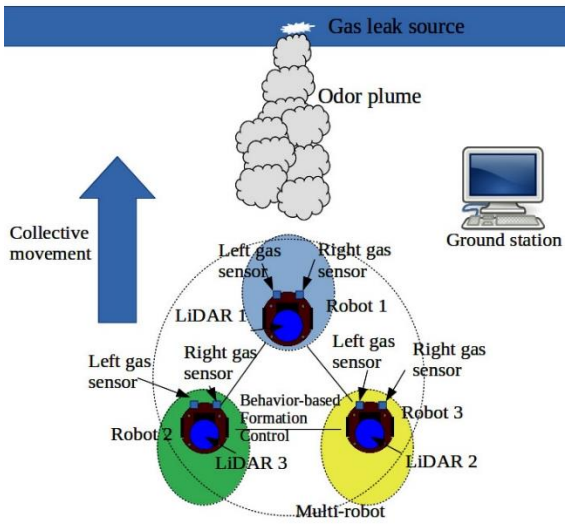

Figure. 1 Robot group system in the search for gas leak sources

2. Proposed method

An overview of the gas leak source tracking robots' cluster system is illustrated in Fig. 1. The robot group consists of three identical robots that move together toward the gas leak source. The three robots move in a V formation with the leader robot in the front position and the follower robots behind the leader robot. Robot positions are determined by 2D Light Detection and Ranging (LiDAR), allowing each robot to have a position relative to the others. To move the formation toward the gas leak source, the robots use behavior-based formation control. Each robot has two gas sensors in the form of a stereo-nose to track gas plumes. The robot's displacement is assisted by two wheels for differential steering. A ground station is placed as a parameter collector obtained from the robot group.

An illustration of the robots' work in tracking gas plumes in groups is shown in Fig. 2. In the first condition, one leader robot is chosen for the group's front position according to Fig. 2 (a). The robot positioned at the front is considered to have the highest fitness value because it is positioned closest to the gas leak source. The greater the gas concentration detected by the robot, the greater the robot's speed in approaching the gas source. The two follower robots will go along with the leader robot's motion direction by maintaining the distance between the robots. When the change in gas plume occurs, the leader robot's perceived gas concentration decreases, and the leader robot's speed decreases until it stops.

The two follower robots that perceive higher gas concentration have the potential to replace the leader's position after one of the follower robots precedes the leader robot.

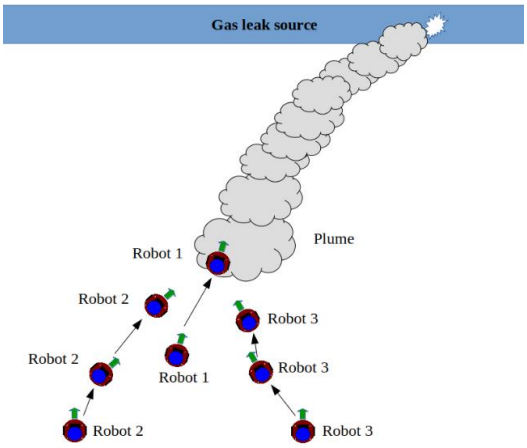

(a)

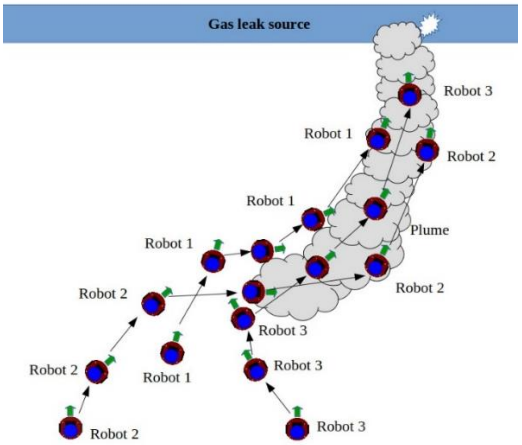

(b)

Figure. 2 Robot group mechanism: (a) the initial trajectory, and (b) the trajectory after the change in gas or odor plume

An illustration of the gas plume tracer's work with changes in formation is shown in Fig. 2 (b).

2.1 Differential steering robot

This study involved a differential steering mobile robot. This is one of the most popular types of robots because of its high movement and maneuvering, as well as low cost [10-11]. The differential steering robot's block diagram is depicted in Fig. 3, while the realization of the robot is shown in Fig. 4. The STM32 microcontroller was used as the main processor in this robot. The speed generated by each wheel was obtained from the robot's behavior toward the data from RPLIDAR A1 and two metal oxide gas sensors. In cartesian coordinates, the robot posture is illustrated in Fig. 5.

The mathematical model of the position φ and orientation γ of the robot i at time k is expressed in Eq. (1), in which x_k^i, y_k^i are positions in Cartesian space. The robot movement speed $\dot{\chi}_k^i$ is expressed in

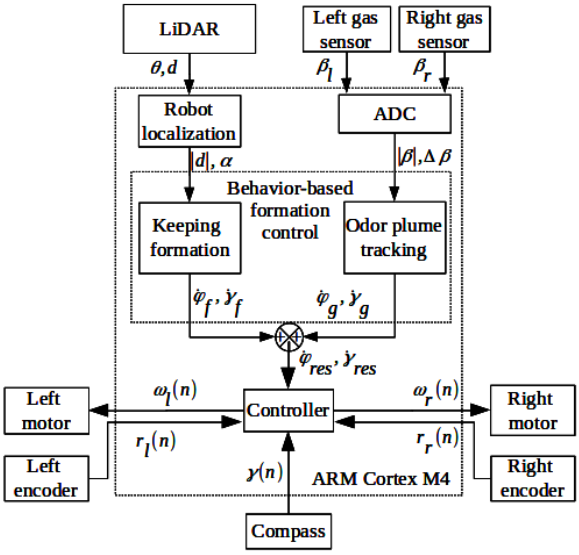

Figure. 3 Differential steering robot block diagram

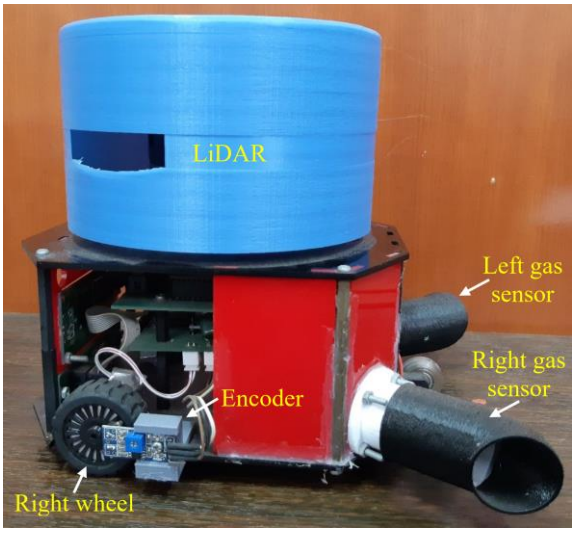

Figure. 4 Realization of the robot

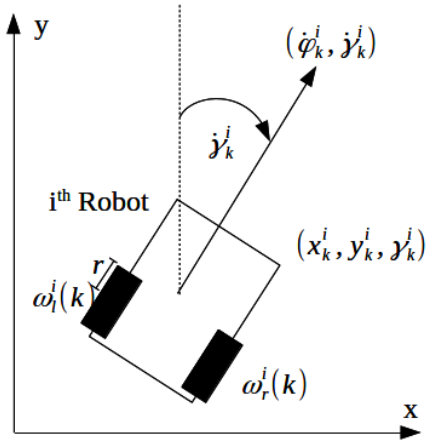

Figure. 5 Robot posture in Cartesian coordinates

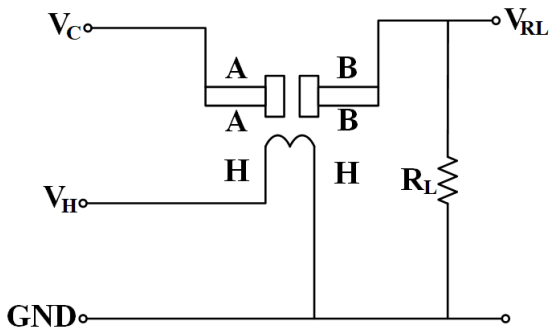

Figure. 6 Signal conditioning circuit for MOS gas sensor

Eq. (2). The robot's speed is a function of the gas concentration and the robot's position which is expressed in Eq. (3) allowing the updated robot position to be expressed in Eq. (4).

$$\chi_k^i = \begin{bmatrix} x_k^i & y_k^i & \gamma_k^i \end{bmatrix}^T \quad (1)$$

$$\dot{\chi}_k^i = \begin{bmatrix} \dot{x}_k^i & \dot{y}_k^i & \dot{\gamma}_k^i \end{bmatrix}^T \quad (2)$$

$$\dot{\chi}_k^i = f(|\beta|, \Delta\beta) + f(|d|, \alpha) \quad (3)$$

$$\chi_{k+1}^i = \chi_k^i + \dot{\chi}_k^i \quad (4)$$

2.2 Stereo-nose

To approach the gas leak source, the robots needed a stereo-nose in which the working principle was to compare the gas concentration between two gas sensors installed in opposite directions as shown in Fig. 4. There are several types of gas sensors, including metal oxide semiconductors (MOS), quartz crystal microbalances (QCM), surface acoustic waves (SAW), electro-chemical cells (EC), and photoionization detectors (PID) [12]. The MOS gas sensor of MQ-2 was used as the sensor in this study because it has a simple signal conditioning circuit as shown in Fig. 6, low cost, and sufficient selectivity and sensitivity.

The MOS sensor's work principles are based on reduction and oxidation reactions when the sensor material interacts with certain gases [13-14]. As a result of the chemical reaction, there was binding and release of free electrons, causing the R_{AB} resistance value on the sensor to change according to the number of gas particles which is expressed in Eq. (5).

$$R_{AB} = R_L \left(\frac{Vc}{V_{RL}} - 1 \right) \quad (5)$$

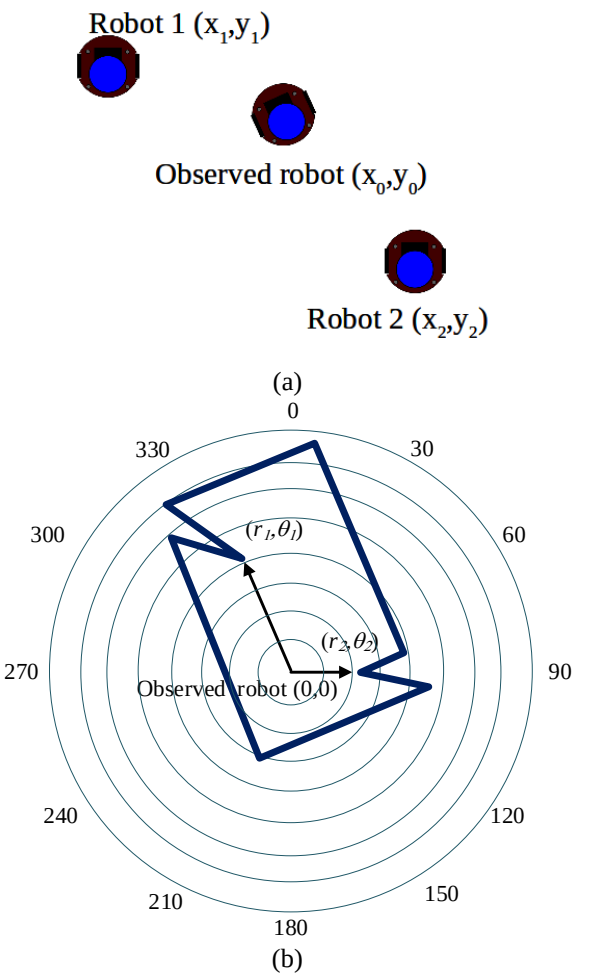

Figure. 7 The 2D LiDAR scanning: (a) position of the robot, and (b) scan results from the observed robot

The gas concentration value β was obtained from the MQ-2 gas sensor datasheet for liquefied petroleum gas, as in Eq. (6).

$$log(\beta) = \frac{\frac{R_{AB}}{R_o} - 0.6}{-4.4} + 4 \quad (6)$$

2.3 Robot localization

The absolute position of a robot is determined by the encoder, while LiDAR is used to obtain the relative position of other robots in a group, allowing each robot to have a different perception of the robot group's position. The localization of the robot group in this study involved two-dimensional LiDAR, and the scanning of the surrounding environment is illustrated in Fig. 7.

The robots' relative positions were determined from the change in distance from the LiDAR scanning results. The robot's position in the polar coordinate consisted of the distance matrix r_i and the angle θ_i from the perception of the robot i, which is expressed in Eq. (7).

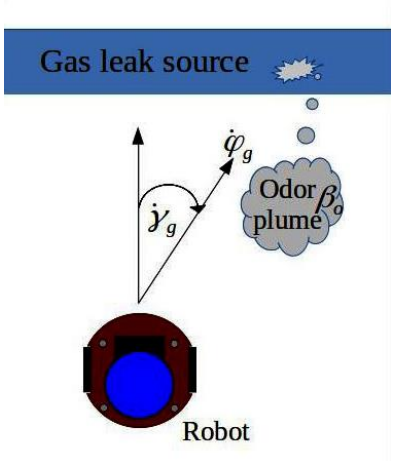

Figure. 8 Robot approaches a gas leak source

$$r_i = [r_i^0 \quad r_i^1 \quad r_i^2]$$
$$\theta_i = [\theta_i^0 \quad \theta_i^1 \quad \theta_i^2] \tag{7}$$

Then, this was converted into cartesian coordinates with the trigonometry equations of Eq. (8).

$$x_i = [x_i^0 \quad x_i^1 \quad x_i^2]$$
$$y_i = [y_i^0 \quad y_i^1 \quad y_i^2] \tag{8}$$

2.4 Formation control

The robots moved together towards the gas leak source; therefore, a control was needed to maintain the shape of the formation. Behavior-based formation control was used in this study because it has an easy algorithm and clear task definitions [8]. In this control, each robot had the same task. In the case of tracking the gas plume with a certain formation, each robot's tasks were defined as tracking the plume and maintaining the formation's shape. Then, the motion speed $\dot{\varphi}$, and the rotation speed $\dot{\gamma}$ from each task, both heading to the gas source (g) and the formation (f) were accumulated and written into Eq. (9).

$$[\dot{\varphi} \quad \dot{\gamma}]^T = \begin{bmatrix} \dot{\varphi}_g & \dot{\varphi}_f \\ \dot{\gamma}_g & \dot{\gamma}_f \end{bmatrix} \begin{bmatrix} 1 \\ 1 \end{bmatrix} \tag{9}$$

2.4.1. Gas plume tracking

Each robot was designed to have the ability to track gas plumes, which is illustrated by Fig. 8. Two gas sensors as the stereo-nose were used as input parameters to control the robots' differential steering. The robots' basic behavior in approaching the gas leak sources is expressed in Eq. (10) and Eq. (11).

$$\dot{\varphi}_g = |\beta| \tag{10}$$

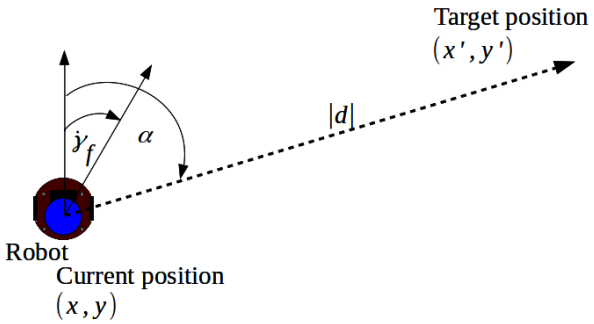

Figure. 9 The robot heading to the target position in the formation

$$\dot{\gamma}_g = \Delta\beta = \beta_r - \beta_l \tag{11}$$

The greater the gas plume concentration received by the robot $|\beta|$, the greater the robot's speed in approaching the gas leak source. The robots' steering speed was taken from the difference in gas concentration between the right sensor β_r and the left gas sensor β_l. Steering speed was directly proportional to the difference in concentration between both sensors.

2.4.2. Keeping formation

The task of maintaining the formation's shape was needed to ensure that no robot lost its way when moving along the gas plume and all robots in the group would go to the same gas leak source. The task of maintaining the formation entailed keeping the same distance between the robots to form an equilateral triangle with the same angle on each side. First, the robot determined the leading robot's position in the group using Eq. (8). Then, it projected the target position where it places itself using Eq. (12), where γ_k^1 was the orientation of the frontmost robot, n was the robot number, and d and α were the distance and angle constant values of 60 cm and 60°, respectively. An illustration of a robot moving toward the target position to maintain the formation shape is shown in Fig. 9.

$$\begin{bmatrix} x' \\ y' \end{bmatrix} = \begin{bmatrix} cos\gamma_k^1 & sin\gamma_k^1 \\ sin\gamma_k^1 & cos\gamma_k^1 \end{bmatrix} \begin{bmatrix} x_1 - (-1^n dcos\alpha) \\ y_1 - dsin\alpha \end{bmatrix} \tag{12}$$

The robot's speed toward the target position was determined by the difference between the two coordinate points. The relationship between the robots' speed and the formation's target position is expressed in Eq. (13). The robot rotation speed was determined by the coordinates of the gas source direction and the robots' orientation, which is expressed in Eq. (14).

$$\dot{\varphi}_f = |d| \quad (13)$$

$$\dot{\gamma}_g = \alpha \quad (14)$$

2.5 Heuristic approach for formation label

Heuristics is an approach to finding a solution to a problem [15]. The resulting solution is close to the best because it is found by identifying the highest fitness value of the group. In this study, the best solution was the robot that detected the highest concentration among the robot groups, indicating the group's maximum speed. As a result, that robot occupied the leading position in the group. From the position information of all robots in the group obtained by the LiDAR, the fitness values could be obtained from the robot position matrix's maximum y-axis value in Eq. (8).

The robot formation is expressed as formation labels of 1, 2, and 3 for blue, yellow, and green, respectively, as shown in Fig. 1. The formation label 1 was given to the leader robot or the robot considered to be the one with the best solution, while the other formation labels were given to the follower robots. In determining the robot that received the label formation 1, the highest fitness value of the robot group had to be identified. Determining formation labels 2 and 3 for follower robots was a challenge because calculations were needed to find the shortest distance and determine the formation label. An illustration of determining the shortest distance is depicted in Fig. 10. The flow chart for determining follower robots' formation labels is shown in Fig. 11. r_1^3 is the distance of follower robot 1 to target position 3, r_1^2 is the distance of follower robot 1 to target position 2, r_2^3 is the distance of follower robot 2 to target position 3, and r_2^2 is the distance of follower robot 2 to target position 2.

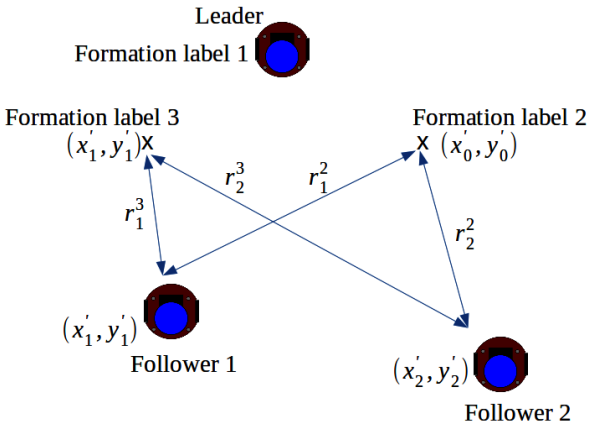

Figure. 10 Follower robot competition in determining formation labels

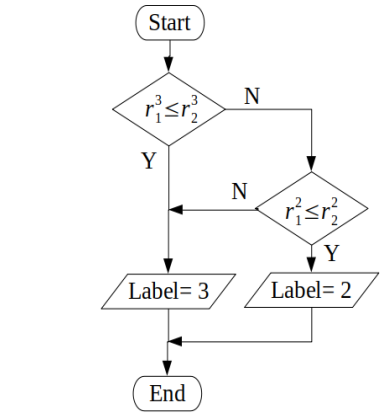

Figure. 11 Flowchart defining formation labels for follower robots

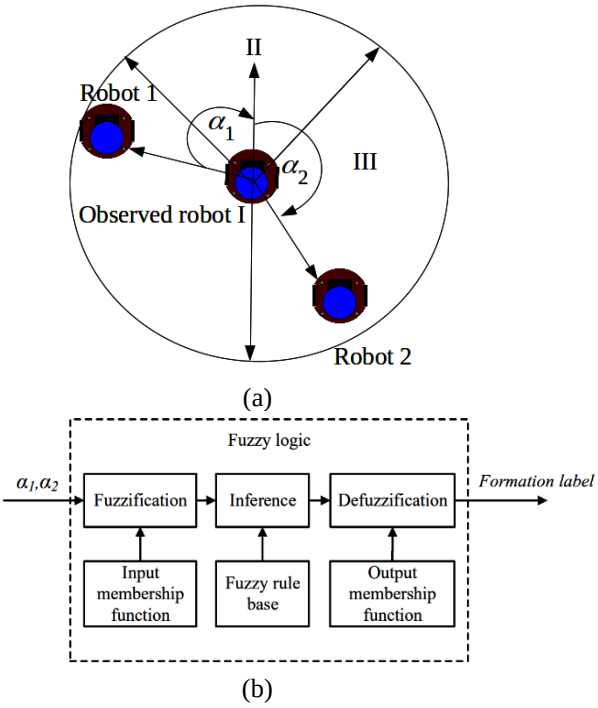

Figure. 12 The method for formation labels: (a) formation determination and (b) fuzzy block diagrams

Table 1. The fuzzy rule for determining formation labels

α2 \ α1	I	II	III
I	1	3	1
II	3	3	2
III	1	2	1

To carry out the function of the flowchart described in Fig. 11, this study used the fuzzy logic method to determine the formation label for each robot. The block diagram of the fuzzy logic is depicted in Fig. 12 with the rules shown in Table 1.

The fuzzy input parameters were generated by the stereo-nose, which consisted of two gas sensors

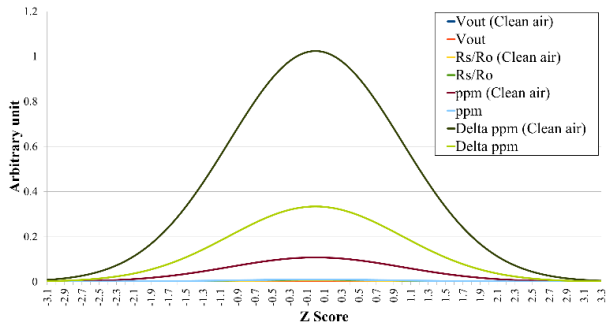

Figure. 13 The normal distribution of gas sensor responses

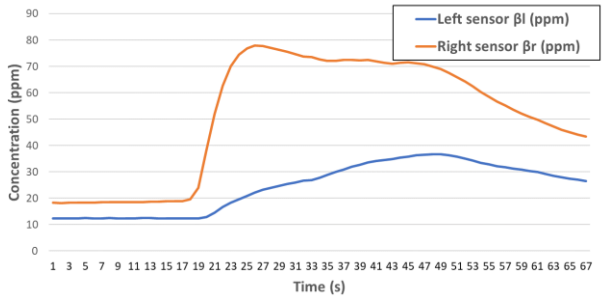

Figure. 14 Stereo-nose gas concentration when the gas source is to the left of the robot

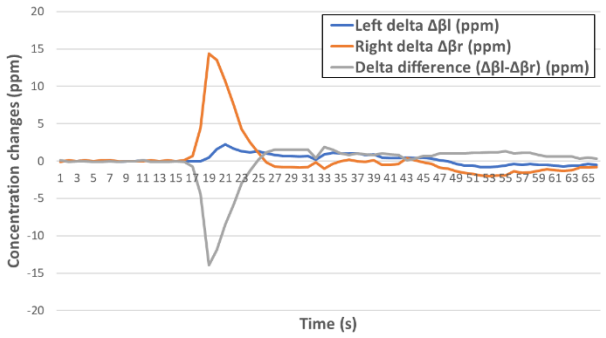

Figure. 15. Stereo-nose gas concentration changes when the gas source is to the left of the robot

located on the robots' right and left sides. Commercial gas sensors did not have the same voltage signal between each other. The normal distribution of gas sensor responses is shown in Fig. 13.

The curve with a higher peak is a good parameter because it has a low standard deviation that produces precision measurements. Based on Fig. 13, the gas concentration amounts in units of parts per million (ppm) and changes in gas concentration were selected as control parameters.

The steering robot was difficult to determine by the difference in gas concentration between the two sensors. Fig. 14 shows two gas sensors' concentration as a stereo-nose when the gas source was placed on the left of the robot.

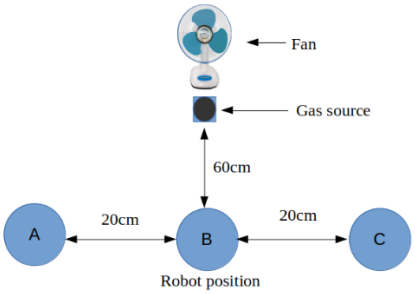

Figure. 16 The stereo-nose testing

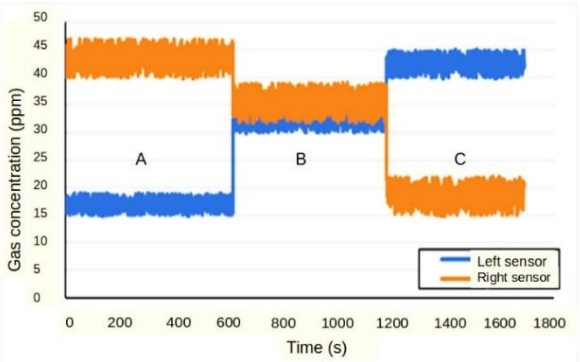

Figure. 17 Response of the stereo-nose to various positions

The more visible feature of the robot steering control was the difference between the concentration changes in the two sensors per unit of time, as shown in Fig. 15.

The robots' behavior was defined as directly proportional to the detected gas concentration. The greater the gas concentration received by the robot, the greater the robot's displacement. This meant that the robot's execution time to reach the gas leak source was minimal.

3. Results and analysis

In the experiments, the gas source was represented by gasoline vapor emitted by an electric fan at a speed of 2 mph. These tests included gas sensors as the stereo-nose, robot localization with LiDAR, formation label determination, and gas plume tracking.

3.1 Stereo-nose

Testing of the stereo-nose was carried out to determine the gas concentration received by the gas sensors for various robot positions, as depicted in Fig. 16. Fig. 17 shows the stereo-nose response against various positions. In the position of A and C, each sensor had a significant difference in gas concentration, while in the position of B, each sensor had a similar value. This test indicated that the stereo-

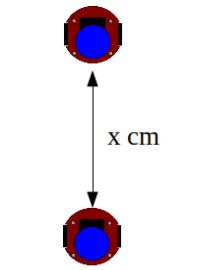

(a)

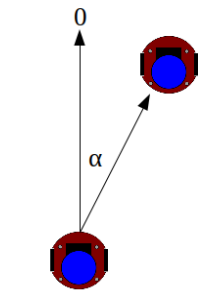

(b)

Figure. 18 Testing the localization of robots with LiDAR which includes measurements of (a) the distance and (b) the angle

Table 2. Distance measurement results

Actual distance (cm)	Measured distance (cm)	Accuracy (%)
30	24.3	81.0
60	54.5	90.8
90	85.8	95.4
120	120.2	98.8
150	149.7	99.8
180	174.1	96.7
210	205.9	98.0
240	236.2	98.4
270	265.5	98.3
300	265.5	88.4
Average		94.7

Table 3. Angular measurement results

Actual angle (º)	Measured angle (º)	Accuracy (%)
0	3.5	99.0
45	43.2	99.5
90	85.8	98.8
135	127.62	97.9
180	175.9	98.8
225	214.1	96.9
270	267.8	99.4
315	326.2	90.7
Average		97.6

nose can be used to steer the robot toward the gas leak source.

Table 4. The fitness value (Fn) and formation label of each robot with a variety of positions

Test of Position	Fn A	Fn B	Fn C	Label A	Label B	Label C
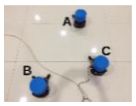	57	0	23	1	3	2
	38	0	37	1	2	3
	128	34	0	1	3	3
	128	65	0	1	2	2
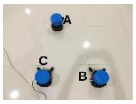	73	0	28	1	2	2
	0	0	60	2	3	1
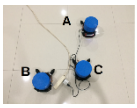	37	0	33	1	3	3
	29	0	73	3	2	1
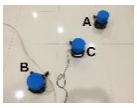	46	0	10	1	3	3
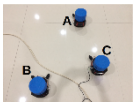	126	0	85	1	3	3

3.2 Robot localization with LiDAR

The robots' localization was tested with LiDAR. This test was carried out on various distances and angles, as depicted in Fig. 18. The localization results with angle and distance variations are shown in Table 2 and Table 3. The distance and angle measurements had an accuracy rate of 94.7% and 97.6%, respectively. All the distance measurements were carried out in the LiDAR measurement range.

3.3 Formation label

Determination of the formation label was carried out with the heuristic approach used in the robot group system, where the leader could change

Table 5. The travel time of the individual robot to find the gas source

Experiment	x (cm)	Travel Time (s)			
		1st	2nd	3rd	Average
No disturbance	120	28.6	56.9	180.0	88.5
	180	46.8	58.8	180.0	95.2
	240	61.3	78.5	180.0	106.6
	300	80.1	151.2	180.0	137.1
With disturbance	120	45.3	141.7	180.0	122.3
	180	99.5	180.0	180.0	153.1
	240	104.1	143.3	180.0	142.5
	300	107.8	144.3	180.0	144.0

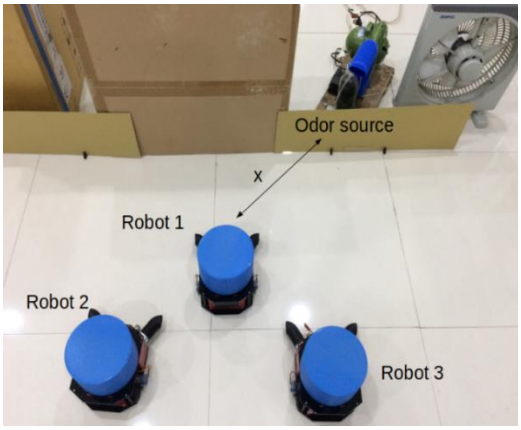

(a)

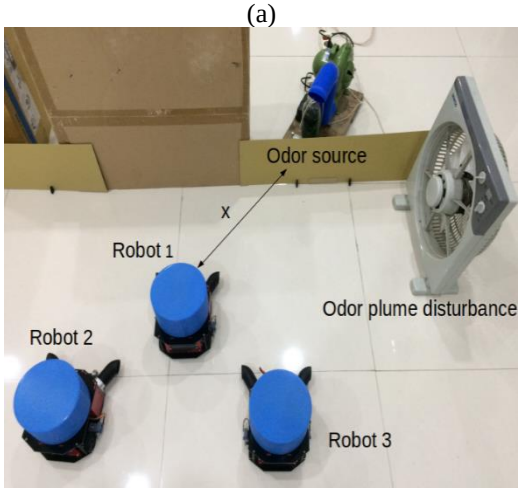

(b)

Figure. 19 Testing scenario of gas plume tracking: (a) without disturbing the airflow and (b) without disturbing the airflow

according to their fitness value. This test was carried out by putting the robots in any position, then observing each robot's fitness value and formation label. The results of this experiment are shown in Table 4.

3.4 Gas plume tracking

In the gas plume tracking test, two scenarios were carried out, namely without the gas plume disturbance and with the addition of the gas plume disturbance. In the test with a disturbance, the second electric fan was turned on five seconds after the robots ran. The test was carried out with a variety of distances x with three repetitions for each distance. In this experiment, the travel time for each test was observed. For robots that failed in tracking, the travel time was at the maximum value of 180 seconds. The gas plume tracking test scenario is illustrated in Fig. 19.

3.4.1. Gas plume tracking without the formation

This test aimed to observe the robots' ability to track the gas plume individually or independently. The swarms of robots did not form a formation during tracking.

The travel time is shown in Table 5. In this test, many travel times were around 180 seconds, which indicates that the robots were unable to move toward the gas source. The robots' trajectories are shown in Fig. 20. Robots 2 and 3 experienced a loss of direction when following the gas plume. On the other hand, the use of a gas plume disturbance in the test extended the robots' travel time in moving toward the gas source because the received gas concentration decreased.

3.4.2. Gas plume tracking with a fixed formation

In this section, the swarm of robots is tracked together while maintaining the fixed formation's shape. The travel time generated by the robots is shown in Table 6. Compared to Table 5, the average travel time in this test was faster by 52.8%. All robots managed to reach the gas source. The trajectories of the robots are shown in Fig. 21.

Table 6 and Fig. 21 show that no robot lost its way in tracking the gas plume. The addition of the gas plume disturbance caused longer tracking travel times.

3.4.3. Gas plume tracking with heuristic approach on the formation

In this section, the swarms of robots tracked the gas leak source using a heuristic approach for the formation, meaning the group's leader could change. The travel time in this test is shown in Table 7, and the robots' trajectories are shown in Fig. 22. The average travel time produced in this test was 62.2% shorter than the results obtained in Table 5. While compared with Table 6, this robot system was 19.4% faster.

The travel time for robots during airflow with and without disturbance had a relatively small difference.

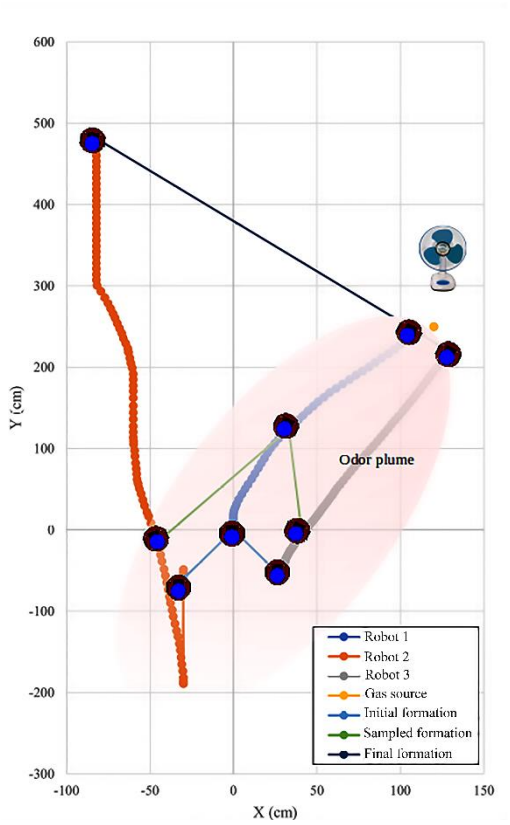

(a)

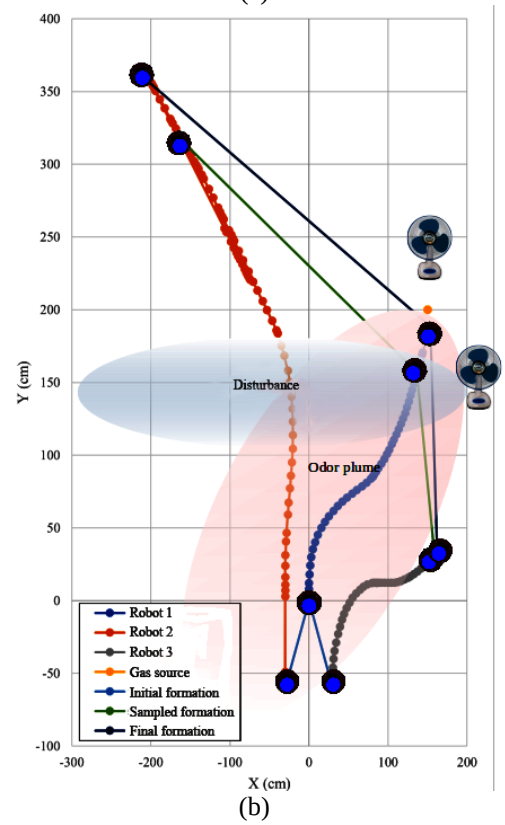

(b)

Figure. 20 The individual robot trajectories: (a) without disturbance and (b) with disturbance

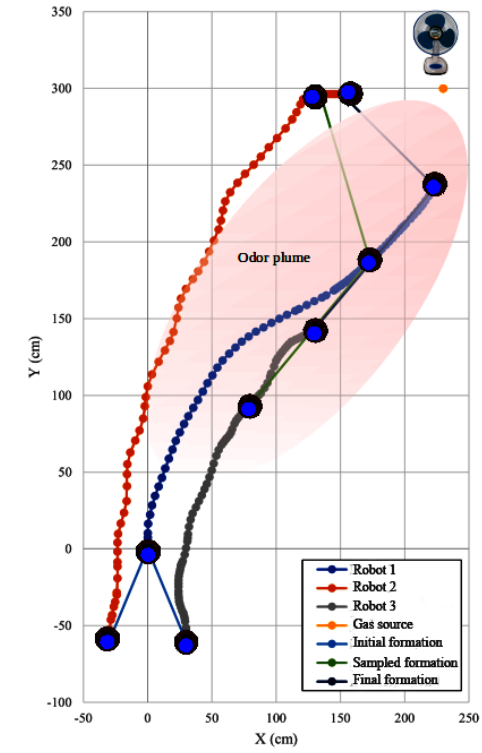

(a)

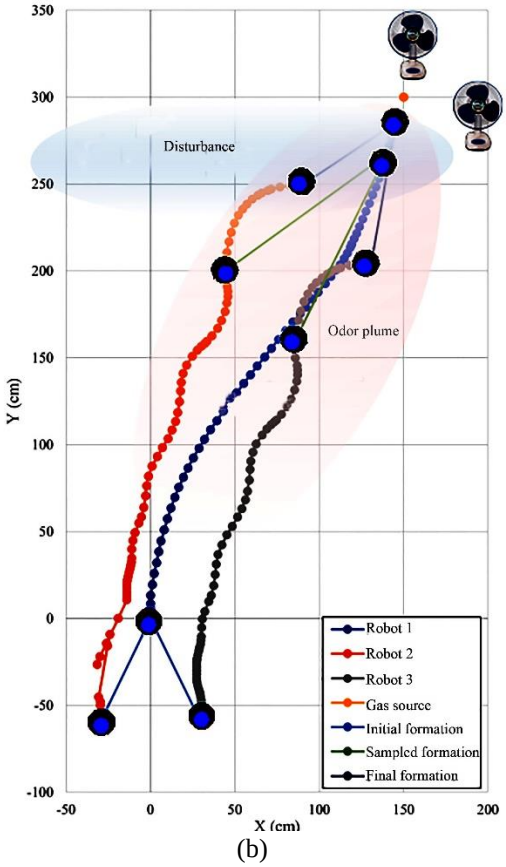

(b)

Figure. 21 The robot trajectories in a fixed formation: (a) without disturbance and (b) with disturbance

The robots' trajectories also show changes in the leader robot. This indicates that the heuristic

Table 6. The travel time of the robots in a fixed formation to find the gas source

Experiment	x (cm)	Travel Time (s)			
		1st	2nd	3rd	Average
No disturbance	120	31.6	33.2	37.4	34.1
	180	38.8	41.2	43.6	41.2
	240	55.7	67.0	70.8	64.5
	300	73.0	78.7	80.5	77.4
With disturbance	120	42.2	42.8	46.6	44.2
	180	47.9	48.4	49.7	48.6
	240	68.7	69.8	71.2	69.9
	300	78.3	81.7	106.7	88.9

Table 7. The travel time of the robots using a heuristic approach to find the gas source

Experiment	x (cm)	Travel Time (s)			
		1st	2nd	3rd	Average
No disturbance	120	28.0	31.6	35.4	31.7
	180	37.0	37.7	37.3	37.3
	240	44.4	48.9	62.0	51.5
	300	51.5	61.0	81.0	64.5
With disturbance	120	25.0	35.0	35.0	31.7
	180	35.0	37.0	37.0	39.0
	240	49.0	49.0	65.0	54.3
	300	53.0	65.0	65.0	61.0

approach in the formation can produce a robust system for gas leak source tracking.

3.5 Comparison of the robot systems' performance

A comparison of the robot systems' performance in finding gas leak sources is shown in Table 8. The parameters include gas sensors, multi robots, disturbances, robot type, localization methods, gas type, and improvement compared to a single robot. Other gas leak source search systems in the literature have not involved disturbances when the mobile robot searches for gas leak sources. The proposed method had the highest improvement when compared to a single robot.

4. Conclusion

This study designed and realized swarms of robots to locate gas leak sources. This robot group consisted of three identical robots, where each robot was equipped with RPLIDAR A1, MQ-2 gas sensors, and STM32 microcontrollers. The experimental results show that this robot group could move collectively and maintain the V formation while tracking gas plumes, even when faced with airflow disturbance. The heuristic method application in the formation guaranteed that the leader robot in the group could change according to its fitness value. The implementation of this method produced a travel time 62.2% shorter than that of single robots, and 19.4% shorter than that of robot groups with a fixed formation. Future studies on robot groups to find gas leak sources should equip robots with wind sensors to determine wind direction. This will allow the robot system to approach the gas source with greater disturbance in air flow conditions outdoors.

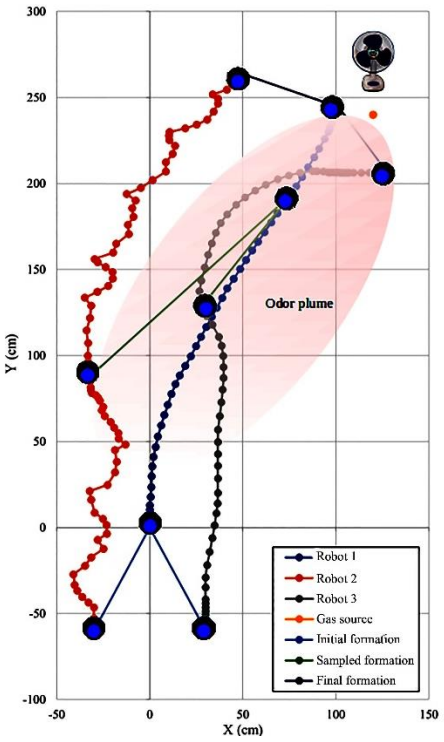

(a)

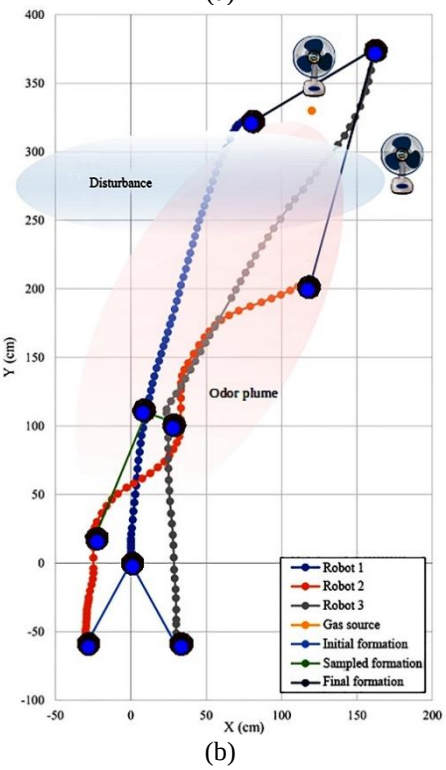

(b)

Figure 22. The robot trajectories using a heuristic approach: (a) without disturbance and (b) with disturbance

Table 8. Comparison of the robot systems' performance in finding gas leak sources

Literature	Gas sensor	Multi robots	With disturbance	Robot type	Localization methods	Gas plume type	The improvement compared to a single robot
Ref [1]	TGS2611	No	No	Mobile robot	Differential steering	Gasoline	-
Ref [2]	MQ-3, MQ-5	Yes	No	Mobile robot	Fuzzy Logic, PSO, and SVM	Alcohol, LPG	No description
Ref [3]	MiCS-5521 CO/VOC	Yes	No	Mobile robot	No description	Ethanol	0.54%
Proposed	MQ-2	Yes	Yes	Mobile robot	Differential steering, PSO, FLC	Gasoline	62.2%

Conflicts of interest

The author(s) declared no potential conflicts of interest with respect to the research, authorship, and/or publication of this article.

Author contributions

For this study, the article author contributions are as follows: "conceptualization and methodology, Dony Hutabarat, Muhammad Rivai, and Muhammad Agung Nursyeha; software, Muhammad Agung Nursyeha; data curation, Sheva Aulia; writing-original draft preparation, Dony Hutabarat; writing-review and editing by Dony Hutabarat and Muhammad Rivai; supervision, Muhammad Rivai, and Djoko Purwanto".

Acknowledgments

The authors would like to thank the Indonesian Ministry of Education, Culture, Research, and Technology for its financial support.

References

[1] W. Helmy, M. Rivai, and T. Mujiono, "Odor Source Searching in Mechanical Turbulent Airflow Using a Mobile Robot", *International Journal of Intelligent Engineering and Systems*, Vol. 13, No. 3, pp. 167–176, 2020, doi: 10.22266/ijies2020.0630.16.

[2] Husnawati, G. F. Fitriana, and S. Nurmaini, "The development of hybrid methods in simple swarm robots for gas leak localization", In: *International Conference on Signals and Systems*, Bali, Indonesia, pp. 197–202, 2017.

[3] J. M. Soares, A. P. Aguiar, and A. M. Pascoal, "A distributed formation-based odor source localization algorithm - Design, implementation, and wind tunnel evaluation", In: *International Conference on Robotics and Automation*, Seattle, WA, USA, pp. 1830–1836, 2015.

[4] M. Rivai, Rendyansyah, and D. Purwanto, "Implementation of fuzzy logic control in robot arm for searching location of gas leak", In: *Proc. of International Seminar on Intelligent Technology and Its Applications*, Surabaya, Indonesia, pp. 69–74, 2015.

[5] T. Ma, S. Liu, and H. Xiao, "Multirobot searching method of natural gas leakage sources on offshore platform using ant colony optimization", *International Journal of Advanced Robotic Systems.*, Vol. 17, No. 5, pp. 1–16, 2020.

[6] T. Jing, Q. H. Meng, and H. Ishida, "Recent Progress and Trend of Robot Odor Source Localization", *IEEJ Transactions on Electrical and Electronic Engineering*, Vol. 16, No. 7. pp. 938–953, 2021.

[7] M. Asenov, M. Rutkauskas, D. Reid, K. Subr, and S. Ramamoorthy, "Active localization of gas leaks using fluid simulation", *IEEE Robotics and Automation Letters*, Vol. 4, No. 2, pp. 1776–1783, 2019.

[8] M. A. Nursyeha, M. Rivai, and D. Purwanto, "LiDAR Equipped Robot Navigation on Behavior-based Formation Control for Gas Leak Localization", In: *Proc. of International Seminar on Intelligent Technology and Its Application*, Surabaya, Indonesia, pp. 89–94, 2020.

[9] S. Hadi, M. Rivai, and D. Purwanto, "Leader-Follower Formation System of Multi-Mobile Robots for Gas Source Searching", *Journal of Physics*, Vol. 1201, No. 1, pp. 1-10, 2019.

[10] D. V. Shabanov, A. V. Kozlovich, and R. R. Valiev, "Autonomous wheeled mobile robot maneuvering in constraint environment. Trajectory tracking quality criteria", *Journal of Physics*, Vol. 1753, No. 1, pp. 1-19, 2021.

[11] A. A. S. Gunawan, William, and B. Hartanto, "Development of Affordable and Powerful

Swarm Mobile Robot Based on Smartphone Android and IOIO board", In: *Proc. of International Conference on Computer Science and Computational Intelligence*, Bali, Indonesia, pp. 342–350, 2017.

[12] J. Jońca, M. Pawnuk, A. Arsen, and I. Sówka, "Electronic Noses and Their Applications for Sensory and Analytical Measurements in the Waste Management Plants—A Review", *Sensors*, Vol. 22, No. 4, pp. 1-32, 2022.

[13] S. Kaaliveetil, J. Yang, S. Alssaidy, Z. Li, Y. Cheng, N. H. Menon, C. Chande, and S. Basuray, "Microfluidic Gas Sensors: Detection Principle and Applications," *Micromachines*, Vol. 13, No. 10, pp. 1–26, 2022.

[14] N. A. Isaac, I. Pikaar, and G. Biskos, "Metal oxide semiconducting nanomaterials for air quality gas sensors: operating principles, performance, and synthesis techniques", *Microchimica Acta*, Vol. 189, No. 5, pp. 1-22, 2022.

[15] Y. F. Yiu, J. Du, and R. Mahapatra, "Evolutionary Heuristic A∗Search: Pathfinding Algorithm with Self-Designed and Optimized Heuristic Function", *International Journal of Semantic Computing*, Vol. 13, No. 1, pp. 5–23, 2019.